Research Article

Nasser Kh. Muhaisen*, Thair Sh. Khayyun, Mustafa Al Mukhtar and Waqed H. Hassan

Forecasting changes in precipitation and temperatures of a regional watershed in Northern Iraq using LARS-WG model

https://doi.org/10.1515/eng-2022-0567 received October 15, 2023; accepted November 15, 2023

Abstract: Regions characterized by an arid or semi-arid climate are highly susceptible to prospective climate change impacts worldwide. Therefore, evaluating the effects of global warming on water availability in such regions must be accurately addressed to identify the optimal operation policy of water management facilities. This study used the weather generator model LARS-WG6.0 to forecast possible variations in precipitation and temperature of the Mosul Dam Reservoir in northern Iraq. Future climate change was predicted using three greenhouse gas emission scenarios (i.e., RCP2.6, RCP4.5, and RCP8.5) for four time intervals (2021–2040, 2041–2060, 2061–2080, and 2081–2100) using five Global climate models (GCMs): CSIRO-Mk3.6.0, HadGEM2-ES, CanESM2, BCC-CSM1-1, and NorESM1-M. The model's calibration and validation were conducted using data from 2001 to 2020 from eight meteorological stations in the study area. The results showed that the weather generator model's performance was outstanding in predicting daily climate variables. The results also showed that the highest increase in maximum and minimum temperatures was 5.70°C in July and 5.30°C in September, respectively, for the future period 2081-2100 under RCP8.5. The highly forecasted minimum and maximum temperatures were extracted from the CanESM2 and HadGEM2-ES GCM models. It was demonstrated that the study region would experience different patterns of precipitation change during the wet seasons in the evaluated periods. Finally, the variations in

precipitation and temperatures in the Mosul dam region would significantly impact the amount of freshwater obtained in these areas due to rising loss rates of evaporation. This could lead to a water shortage and mismanagement of the sustainable operations of the dam.

Keywords: Mosul dam, arid and semi-arid climate, GCM models, RCP, weather generator model

1 Introduction

Climate change is a paramount environmental concern currently confronting the world [1]. Furthermore, climate change is defined as a spatial and temporal alteration in the distribution of rainfall and snowfall patterns within a specific geographical area [2]. Climate change can seriously affect many essential aspects of the global economy, including water resources, agricultural sector, energy production, and tourism [3–5]. Due to the high concentration of greenhouse gases resulting from fossil fuels, human activities, and land use, global warming is responsible for changing global climate [6].

The Intergovernmental Panel on Climate Change (IPCC) 2014 approved the RCP 2.6, 4.5, 6, and 8.5 as inferential greenhouse emissions in the present century based on demographics, financial habits, landscape circumstances, energy utilization, and climate policy. The Coupled Model Intercomparison Project, also known as CMIP, is a structure for a collaborative effort established to enhance the development of Global Climate Models (GCMs) [7]. The five-phase Coupled Model Intercomparison Project, also known as CMIP5, has more characteristics than the older iteration in the carbon cycle simulation, anticipating the system in onedecade steps and identifying the reaction of climate models [8,9]. The GCMs provided predictions of the climate worldwide, allowing policymakers to adjust better strategies to address the consequences of global warming based on the information supplied by the GCMs. GCMs use the complexity of the global system to produce valuable results at the

Thair Sh. Khayyun: Civil Engineering Department, University of Technology-Iraq, Baghdad, 10066, Iraq, e-mail: 40073@uotechnology.edu.iq

Mustafa Al Mukhtar: Civil Engineering Department, University of Technology-Iraq, Baghdad, 10066, Iraq, e-mail: mmalmukhtar@gmail.com **Waqed H. Hassan:** College of Engineering, University of Warith Al-Anbiyaa-Iraq, Karbala, 56001, Iraq, e-mail: waqed.hammed@uowa.edu.iq

^{*} Corresponding author: Nasser Kh. Muhaisen, Civil Engineering Department, University of Technology-Iraq, Baghdad, 10066, Iraq, e-mail: bce.19.82@grad.uotechnology.edu.iq

international, hemispheric, and continental levels. However, these global processes cannot be shown at the local sub-grid level [10]. GCMs are extensively used tools to determine the impact of global warming; however, because of their loose geographic resolution, their direct application to the sustainable management of resources at the regional or local scale is limited [11]. The downscaling approaches are necessary for increasing the geographic resolution of GCMs from a coarse level to a satisfactory level, which is required for their direct application on a local or regional scale [12]. The two downscaling techniques that are most commonly used are statistical downscaling and dynamic downscaling. Both of these methods connect the coarse resolution of GCMs to local environmental variables [13].

In previous research works, statistical downscaling methods were chosen because they are more convenient to use, have more computing power than dynamic downscaling techniques, and are cheaper. These are the three main reasons why statistical downscaling methods were chosen. Two frequently employed software tools for climate predictions and the downscaled analysis of past and future climate data are the Stochastic Weather Generator (Long Ashton Research Station Weather Generator; LARS-WG), Climate Generator (CLIGEN), and Statistical Downscaling Models (SDSM) [14,15]. SDSM can also analyze past climate data [16]. The LARS-WG model is a type of random weather generator. It is one of the most widespread models created to assess climate change's effects. It has been committed to investigating various environmental circumstances, during which it has performed admirably compared to other generators [1].

There are several studies on the world used the results from various GCMs to investigate the effect of global warming on the water resources [17-19]. For example, Osman et al. [3] studied the effect of climate changes on Baghdad City in Iraq based on two scenarios of the seven general circulation model and concluded that the trend of precipitation increased in the autumn and winter seasons while the trend decreased in the spring season for all periods considered in the research. Mohammed and Scholz [20] utilized LARS-WG to study the potential impacts of global warming on northern Iraq's Lower Zab River watershed. Compared to the reference period, the findings showed that the maximum temperatures are expected to rise from 3.17 to 3.70°C between 2046 and 2065, while the minimum temperatures are expected to increase from 3.02 to 3.33°C during that same period.

Additionally, Mohammed et al. [1] investigated the climate change impact on southern Iraq by utilizing the LARS-WG model based on two emission scenarios of the five general circulation model, and annual minimum and maximum temperatures are projected to rise approximately 6°C under RCP8.5 and 1.5°C under RCP4.5 by the end of this century, across all survey sites. The outcomes also reveal that the five GCMs have conflicting projections for precipitation decline patterns.

The novelty of this study is that it provides a conceivable exploration of climate change's impact on northern Iraq's water resources, thereby aiding in decision-making processes related to water resource management, land-use planning, and infrastructure development. In this study, LARS-WG 6.0 was utilized to predict precipitation, minimum, and maximum temperatures for Northern Iraq (Mosul Dam Watershed) over four periods: 2021–2040, 2041–2060, 2061–2080, and 2081–2100. Five CMIP5 models, i.e., CanESM2, CSIRO_Mk3.6, HadGEM2-ES, NorESM1-M, and BCC-CSM1-1 were applied considering three emission scenarios of RCP2.6, RCP4.5, and RCP8.5.

2 Study area and data

The Tigris River, originating in the Taurus Mountains of eastern Turkey approximately 25 km southeast of Elazig and about 30 km away from the source of the Euphrates, spans a length of 1,800 km. This study was focused on the Tigris River basin, which is located between latitude 36°35' 20" to 37°48'00 N and longitude 41°46'33" to 43°29'17" as illustrated in Figure 1. The area of the Mosul Dam watershed is 11,108 km², about 48% of which is located within the Iraqi borders, 44% in Turkey, and 8% in Syria. Climate stations in this region recorded the highest temperature in August, 46°C, while the lowest was in January. The rainy season starts in October and continues until May. The annual rainfall in this region is more than 1,000 mm [21]. This study selected eight meteorological stations to investigate the forthcoming precipitation and temperature patterns, as presented in Table 1. The Climate Hazards Group Infrared Precipitation with Station data and National Aeronautics and Space Administration were consulted to obtain historical data on daily precipitation and maximum and minimum temperatures. These two sources of historical data were collected from two different websites. The weather generator model was calibrated and validated using daily climate data covering two decades, extended from 2001 to 2020.

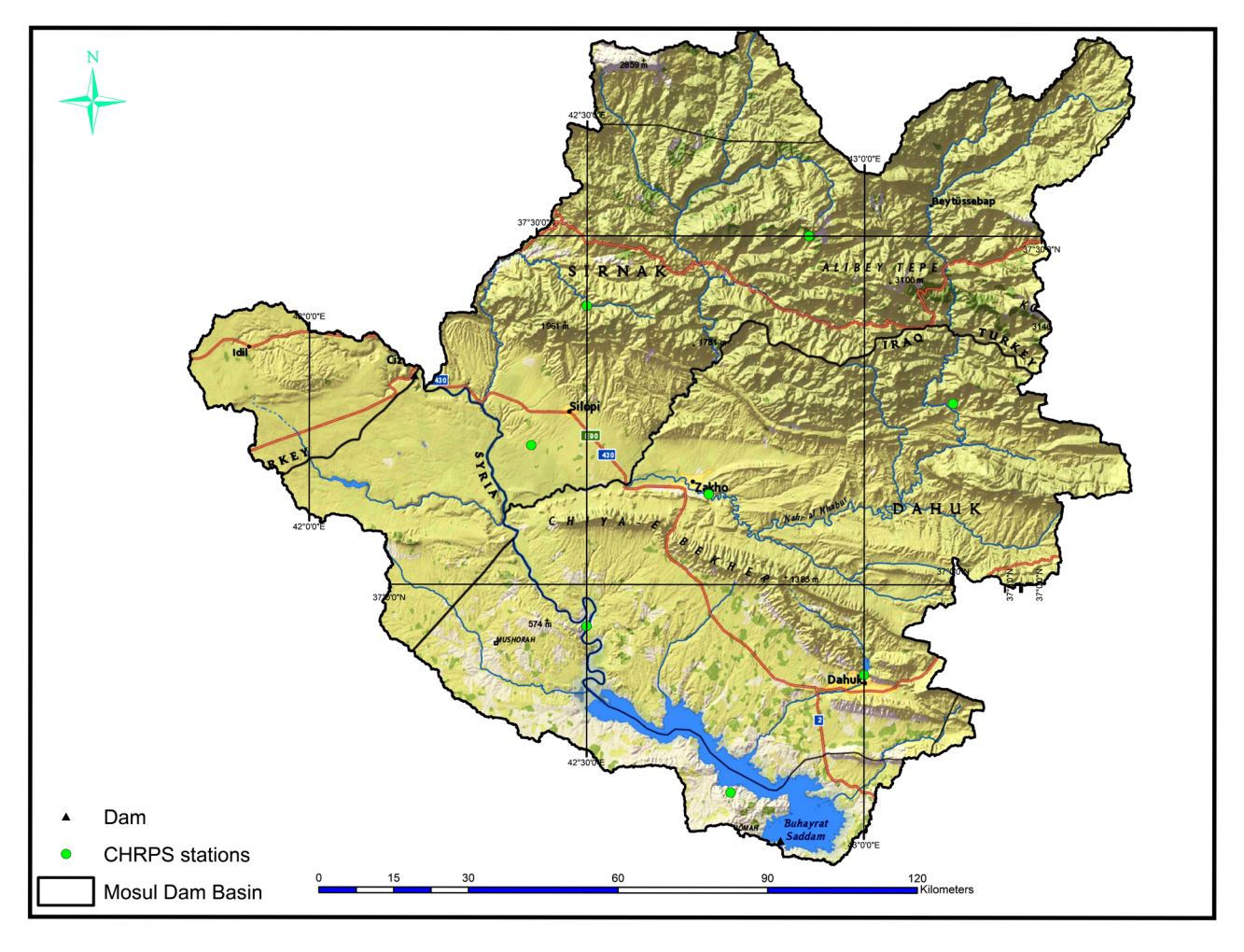


Figure 1: Location of the study area and meteorological stations within it.

Table 1: Geographical coordinates of the selected meteorological stations

Station name	Lat.	Long.	Length of record	Location
Station 1	37°08′00	42°43′12″	2001–2020	Iraq
Station 2	36°52′12″	43°00′00″	2001-2020	Iraq
Station 3	37°15′36″	43°10′00″	2001-2020	Iraq
Station 4	37°30′00″	42°54′00″	2001-2020	Turkey
Station 5	37°24′00″	42°30′00″	2001-2020	Turkey
Station 6	37°12′00″	42°24′00″	2001-2020	Turkey
Station 7	36°57′00″	42°30′00″	2001-2020	Iraq
Station 8	36°42′00″	42°45′00″	2001–2020	Iraq

3 Methodology

3.1 Overview of the LARS-WG model

The LARS-WG is a randomized weather generator that can reproduce weather data at a particular location [22-24]

under present and future climate conditions. These data are presented in the format of daily time series for several different climate variables, including precipitation measured in millimeters, maximum and minimum temperatures measured in °C, and solar radiation. The initial development of stochastic weather generators was motivated primarily by two objectives:

- 1. Develop a methodology that enables the generation of synthetic weather time series, possessing statistical characteristics that closely match the historical statistics at a specific location. The generated time series should also have sufficient length to assess risks in environmental or agricultural contexts.
- 2. For offering a technique for expanding the generation of weather time series to locations that have not been observed by using extrapolation of the weather generator parameters received. Executing the models in nearby locations will extend the simulation to areas that have not been followed.

LARS-WG applies a semi-empirical distribution, the cumulative probability distribution function, to estimate the distributions of dry and moist sequences of daily precipitation and maximum and minimum temperatures. This allows for a more accurate representation of the cumulative probability distribution function. So, to determine the value of the climatic variable v_i , which corresponds to the probability p_i for each climatic variable v, the following formula is used:

$$v_i = \min[v : P(v_{obs} \le v) \ge p_i] i = 0, ..., n,$$
 (1)

$$v_0 = \min\{v_{\text{obs}}\},\tag{2}$$

$$v_n = \max\{v_{\text{obs}}\}. \tag{3}$$

The probability, denoted as P(), relies on the historical observation $\{v_{\rm obs}\}$. For each climatic variable, fixed values, p_0 and $p_{\rm n}$, are established as $p_0=0$ and $p_{\rm n}=1$, respectively, with corresponding values of v_0 and v_n representing the variable's values at the start and end of the intervals. The climatic variable can accurately approximate extreme values by assigning some p_i near zero for significantly low values and near one for extremely high values. The remaining p_i values are evenly distributed across the probability scale.

Due to the relatively high probability of experiencing very low daily precipitation (less than 1 mm) and the minimal impact of such low precipitation on the output of a process-based effect model, only two values were utilized: $v_1 = 0.5$ mm and $v_2 = 1$ mm. The associated probabilities were computed as $p_i = P(v_{obs} \ v_i)$ for i = 1 and 2. This approach is based on the fact that the daily precipitation probabilities being insufficient, i.e., less than 1 mm, is comparatively high in most cases. Additionally, such little precipitation has minimal impact on the result of a processbased effect model. For constructing Synthetic Exceedance Distributions representing wet and dry series, two values close to 1 were employed: $p_{n-1} = 0.99$ and $p_{n-2} = 0.98$. These values were chosen to account for extremely long dry and wet periods. Regarding minimum and maximum temperatures, two values close to 0 and two values close to 1 were utilized, respectively. This choice allows the model to encompass extremely low to extremely high temperatures.

The sixth version of LARS-WG6, developed and published in 2018, incorporates climatic forecasts from 19 GCMs utilized in the IPCC's (AR5) report, known as CMIP5 models. For this particular study on climate change, five models described in Table 2 were selected to forecast changes in precipitation and maximum and minimum temperatures. This reduced the overall uncertainty associated with GCMs.

Future precipitation, minimum, and maximum temperatures were determined by LARS-WG6.0 based on daily historical data of these climate parameters from a particular location for both the prospect distribution of climate parameters and their relations.

3.2 Performance criteria of the model

This study applied a non-parametrized Kolmogorov-Smirnov (K-S) statistical test to evaluate the model's performance. It measures whether the seasonal distributions of the series of wet and dry days and the daily distributions of precipitation obtained from observations and simulations are equal. This test provides a p-value, which is utilized to decide whether to agree or disagree with the assumption that the two sets of data were derived from an identical distribution. High and low values of (K-S) and (p-value) statistics indicate that the model is unlikely because the acquired data are inaccurate and cannot be used to evaluate the model. Katz et al. [25] considered a value of 0.01 for the parameter p to be a reasonable range for the model outputs. According to Mohammed and Hassan [1], the model was considered to have a perfect fit when the pvalue was equal to 1, and it was supposed to have a very good fit when the p-value was more significant than 0.7 but smaller than 1.0. When the p-value was less than 0.7 but greater than 0.4, it was determined that the model had a good fit; on the other hand, it was determined that the model had a poor fit when the p-value fell within the range of 0-0.4. This statistical index is insufficient to assess the model calibration and validation, so, in this study, three

Table 2: Five GCM models used in this study

No.	GCMs' name	Resolution
1	Canadian Center for Climate Modeling and Analysis, Canada (CanESM2)	2.79° × 2.81°
2	Commonwealth Scientific and Industrial Research Organization, Australia (CSIRO-Mk3.6)	1.8° × 1.8°
3	Met Office Hadley Center, United Kingdom (HadGEM2-ES)	1.25° × 1.87°
4	Norwegian Climate Center, Norway (NorESM1-M)	1.89° × 2.5°
5	Beijing Climate Center, China (BCC-CSM1-1)	2.8° × 2.8°

Table 3: Assessment of the LARS-WG model according to the seasonal wet and dry distribution series

Season	Wet/dry	N	K-S	<i>P</i> -value	Assessment	Season	Wet/dry	N	K-S	<i>P</i> -value	Assessment
		9	Station 1						Station 2		
DJF	Wet	12	0.12	0.7384	Very good	DJF	Wet	12	0.05	1.00	Perfect
DJF	Dry	12	0.05	1.00	Perfect	DJF	Dry	12	0.08	1.00	Perfect
MAM	Wet	12	0.04	1.00	Perfect	MAM	Wet	12	0.04	1.00	Perfect
MAM	Dry	12	0.10	0.99	Very good	MAM	Dry	12	0.08	1.00	Perfect
JJA	Wet	12	0.17	0.71	Very good	JJA	Wet	12	0.08	0.97	Very good
JJA	Dry	12	0.17	0.82	Very good	JJA	Dry	12	0.18	0.80	Very good
SON	Wet	12	0.05	1.00	Perfect	SON	Wet	12	0.05	1.00	Perfect
SON	Dry	12	0.05	1.00	Perfect	SON	Dry	12	0.06	1.00	Very good
		S	tation 3						Station 4		
DJF	Wet	12	0.03	1.00	Perfect	DJF	Wet	12	0.05	1.00	Perfect
DJF	Dry	12	0.07	1.00	Perfect	DJF	Dry	12	0.07	1.00	Perfect
MAM	Wet	12	0.03	1.00	Perfect	MAM	Wet	12	0.05	1.00	Perfect
MAM	Dry	12	0.07	1.00	Very good	MAM	Dry	12	0.05	1.00	Perfect
JJA	Wet	12	0.79	0.00	Poor	JJA	Wet	12	0.68	0.00	Poor
JJA	Dry	12	0.17	0.79	Very good	JJA	Dry	12	0.17	0.80	Very good
SON	Wet	12	0.05	1.00	Perfect	SON	Wet	12	0.06	1.00	Perfect
SON	Dry	12	0.07	1.00	Perfect	SON	Dry	12	0.08	1.00	Perfect
	Station 5								Station 6		
DJF	Wet	12	0.08	1.00	Very good	DJF	Wet	12	0.05	1.00	Perfect
DJF	Dry	12	0.06	1.00	Perfect	DJF	Dry	12	0.09	1.00	Very good
MAM	Wet	12	0.03	1.00	Perfect	MAM	Wet	12	0.06	1.00	Perfect
MAM	Dry	12	0.08	1.00	Very good	MAM	Dry	12	0.08	1.00	Perfect
JJA	Wet	12	0.40	0.20	Poor	JJA	Wet	12	0.30	0.60	Good
JJA	Dry	12	0.16	0.86	Very good	JJA	Dry	12	0.14	0.92	Very good
SON	Wet	12	0.02	1.00	Perfect	SON	Wet	12	0.02	1.00	Perfect
SON	Dry	12	0.07	1.00	Perfect	SON	Dry	12	0.07	1.00	Perfect
		9	Station 7						Station 8		
DJF	Wet	12	0.03	1.00	Perfect	DJF	Wet	12	0.05	1.00	Perfect
DJF	Dry	12	0.09	1.00	Perfect	DJF	Dry	12	0.06	1.00	Perfect
MAM	Wet	12	0.03	1.00	Perfect	MAM	Wet	12	0.04	1.00	Perfect
MAM	Dry	12	0.09	1.00	Perfect	MAM	Dry	12	0.08	1.00	Perfect
JJA	Wet	12	0.06	1.00	Perfect	JJA	Wet	12	0.04	1.00	Perfect
JJA	Dry	12	0.27	0.41	Good	JJA	Dry	12	0.17	0.75	Very good
SON	Wet	12	0.07	0.96	Very good	SON	Wet	12	0.03	1.00	Perfect
SON	Dry	12	0.06	1.00	Perfect	SON	Dry	12	0.08	1.00	Perfect

other statistical parameters were used to make the calibration and validation processes of the LARS-WG model, i.e., the coefficient of determination (R^2) , the Nash–Sutcliffe (NS), and the root mean square error (RMSE) to the standard deviation of observed data (STDobs) ratio (RSR). These statistical parameters are used to compare the simulated results with the actual results of the observed data. The coefficient of determination (R^2) measures how efficiently the model duplicated observed outcomes. The values of R^2 range from zero to one, and better model performance is when the value of R^2 is closer to one, as in previous literature [26,27]

A Nash-Sutcliffe efficiency (N_{SE}) value equal to or greater than zero signifies that the simulated value provides more accurate predictions of the concerned component than the mean observed value. On the other hand, an $N_{\rm SE}$ value of one signifies the attainment of ideal modeling. The N_{SE} serves as a measure to compare the variation between the measured and modeled data against a best-fit line with a 1:1 ratio.

The ratio between the RMSE and the standard deviation of the observed data serves as a statistical criterion for error evaluation. Hence, a simulation is acceptable if the RSR value is below 0.5, as in the study by Moriasi et al. [28]. These statistical parameters are determined from the following equations:

$$R^{2} = \frac{\left[\sum_{i=1}^{N} (Q_{i} - Q_{a})(M_{i} - M_{a})\right]^{2}}{\sum_{i=1}^{N} (Q_{i} - Q_{a})^{2} \sum_{i=1}^{N} (M_{i} - M_{a})^{2}},$$
(4)

 Table 4: Assessment of the LARS-WG model according to the fitting of monthly precipitation

Month	N	K-S	<i>P</i> -value	Assess.	Month	N	K-S	<i>P</i> -value	Assess.
		Station	1		Station 2				
J	11.5	0.104	0.9904	Very good	J	11.5	0.065	1	Perfect
F	11.5	0.117	0.9872	Very good	F	11.5	0.091	0.9936	Very good
M	11.5	0.0656	1	Perfect	M	11.5	0.078	0.9968	Very good
Α	11.5	0.1062	0.991	Very good	Α	11.5	0.0576	1	Perfect
M	11.5	0.1126	0.9792	Very good	M	11.5	0.117	0.9384	Very good
J	11.5	0.3742	0.197	Poor	J	11.5	0.3742	0.197	Poor
J	11.5	0.435	0.017	Poor	J	11.5	1	0	Poor
Α	11.5	0.6002	0.0012	Poor	Α	11.5	0.783	0	Poor
S		No pred	ipitation		S	11.5	0.3476	0.16	Poor
0	11.5	0.091	0.9936	Very good	0	11.5	0.1774	0.8176	Very good
N	11.5	0.117	0.9388	Very good	N	11.5	0.1482	0.903	Very good
D	11.5	0.0974	0.9956	Very good	D	11.5	0.0856	0.9964	Very good
		Station	3	, ,			Station	4	
J	11.5	0.065	1	Perfect	J	11.5	0.091	0.9936	Very good
F	11.5	0.065	1	Perfect	F	11.5	0.065	1	Perfect
M	11.5	0.065	1	Perfect	M	11.5	0.065	1	Perfect
Α	11.5	0.0858	0.9954	Very good	Α	11.5	0.0704	1	Perfect
M	11.5	0.1518	0.9152	Very good	M	11.5	0.1446	0.9276	Very good
J	11.5	0.261	0.359	Poor	J	11.5	0.1408	0.909	Very good
J	11.5	0.5044	0.0134	Poor	J	11.5	0.8524	0.0004	Poor
Α	11.5	0.3824	0.0536	Poor	Α	11.5	1	0	Poor
S	11.5	0.2526	0.4444	Good	S	11.5	0.2128	0.61	Good
0	11.5	0.104	0.953	Very good	0	11.5	0.0892	0.993	Very good
N	11.5	0.1022	0.992	Very good	N	11.5	0.117	0.9388	Very good
D	11.5	0.0978	0.995	Very good	D	11.5	0.0764	0.9962	Very good
		Station	5	, ,	Station 6				
J	11.5	0.143	0.9324	Very good	J	11.5	0.078	0.9968	Very good
F	11.5	0.104	0.9904	Very good	F	11.5	0.078	0.9968	Very good
M	11.5	0.065	1	Perfect	M	11.5	0.0668	1	Perfect
Α	11.5	0.0646	1	Perfect	Α	11.5	0.0942	0.9898	Very good
M	11.5	0.1692	0.8362	Very good	M	11.5	0.1182	0.9852	Very good
J	11.5	0.3824	0.0536	Poor	J	11.5	0.523	0.216	Poor
J	11.5	1	0	Poor	J		No pre	cipitation	
Α	11.5	0.6696	0	Poor	Α		No pre	cipitation	
S	11.5	0.3564	0.1096	Poor	S	11.5	0.609	0	Poor
0	11.5	0.077	1	Perfect	0	11.5	0.1306	0.9614	Very good
N	11.5	0.091	0.9936	Very good	N	11.5	0.117	0.9872	Very good
D	11.5	0.0794	0.9952	Very good	D	11.5	0.0924	0.9936	Very good
		Station			Station 8				
J	11.5	0.091	0.9936	Very good	J	11.5	0.104	0.9904	Very good
F	11.5	0.091	0.9936	Very good	F	11.5	0.065	1	Perfect
M	11.5	0.0654	1	Perfect	M	11.5	0.065	1	Perfect
Α	11.5	0.0628	1	Perfect	Α	11.5	0.0772	0.9968	Very good
M	11.5	0.0874	0.9964	Very good	M	11.5	0.0714	1	Perfect
J	11.5	0.5188	0.0094	Poor	J	11.5	0.534	0.203	Poor
j		No pred	ipitation		J No precipitation				
A			ipitation		A No precipitation				
S	11.5	0	1	Perfect	S No precipitation				
0	11.5	0.1224	0.988	Very good	0	11.5	0.1096	0.9512	Very good
N	11.5	0.1592	0.828	Very good	N	11.5	0.134	0.9516	Very good
D	11.5	0.062	1	Perfect	D	11.5	0.0928	0.9964	Very good

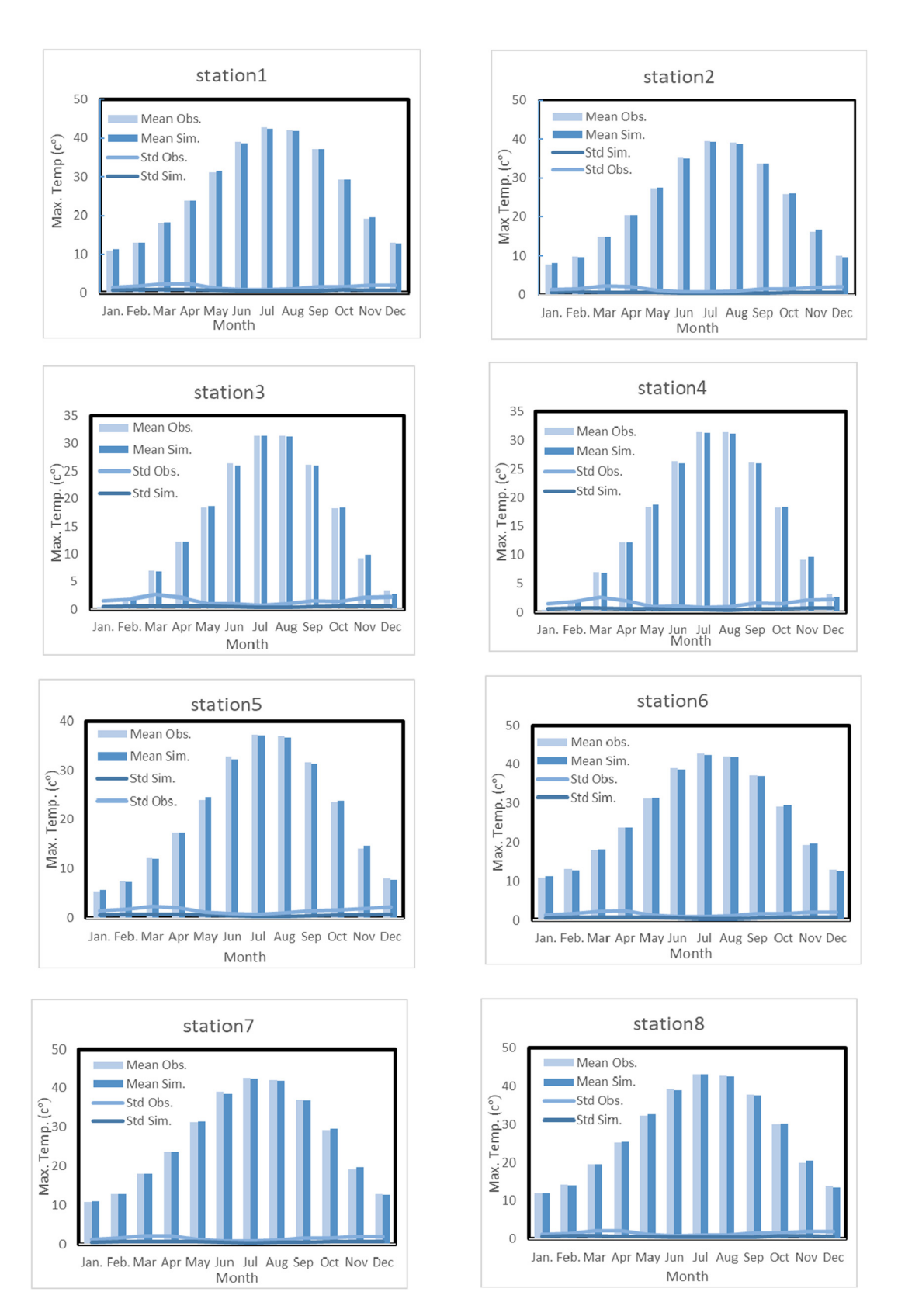
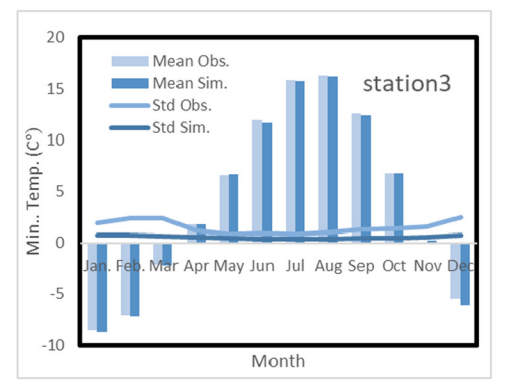
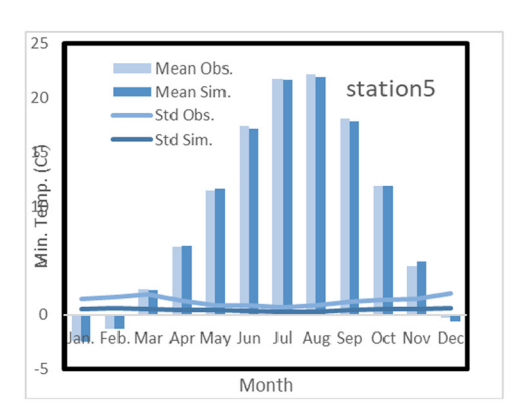
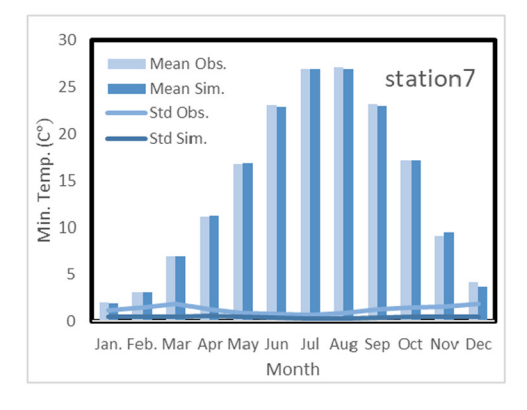


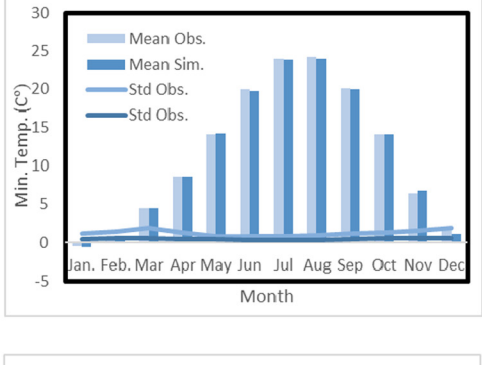
Figure 2: Comparison between the monthly and standard deviation of two series for maximum and minimum temperatures, and precipitation, respectively.



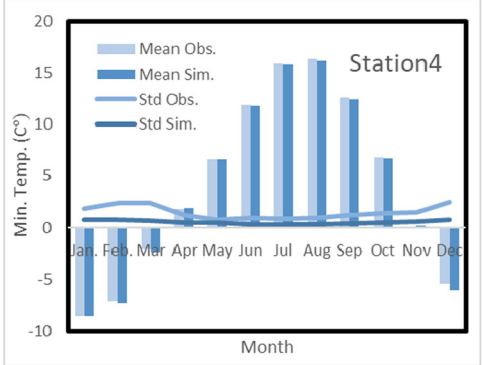


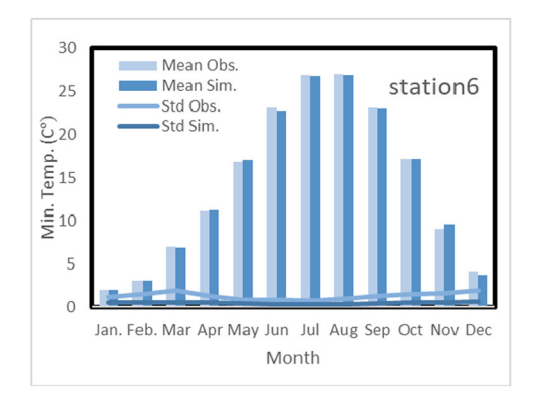






station2





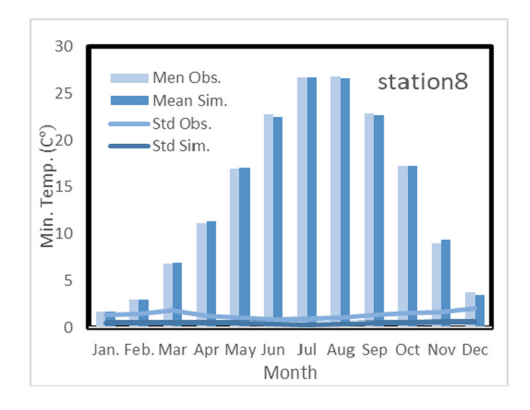
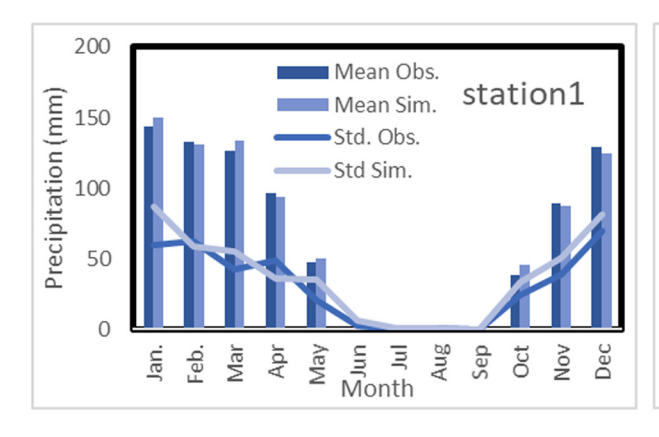
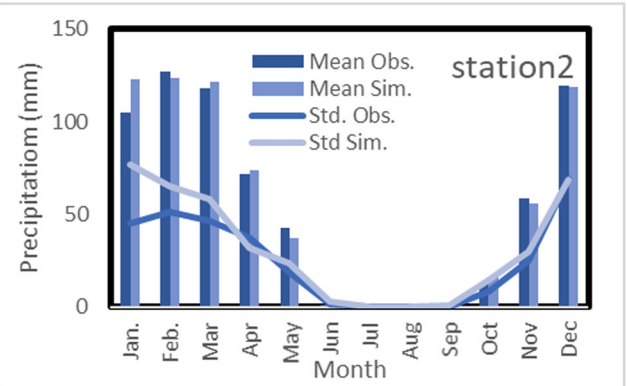
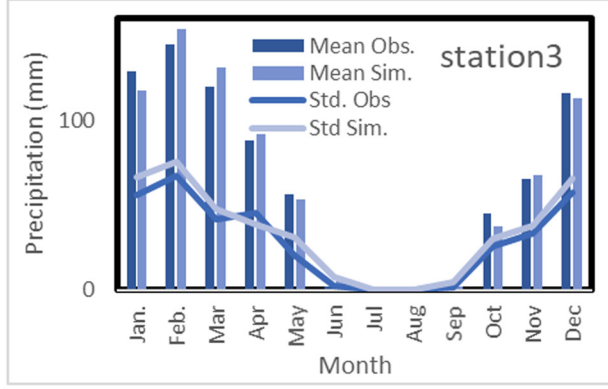


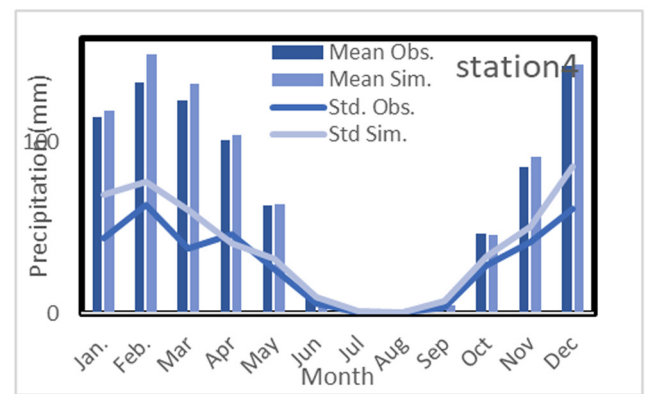
Figure 2: (Continued)

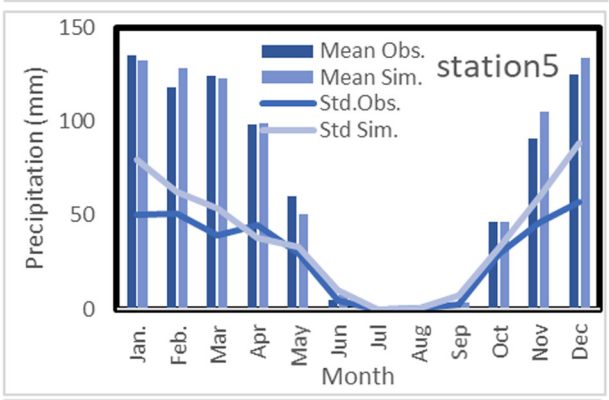


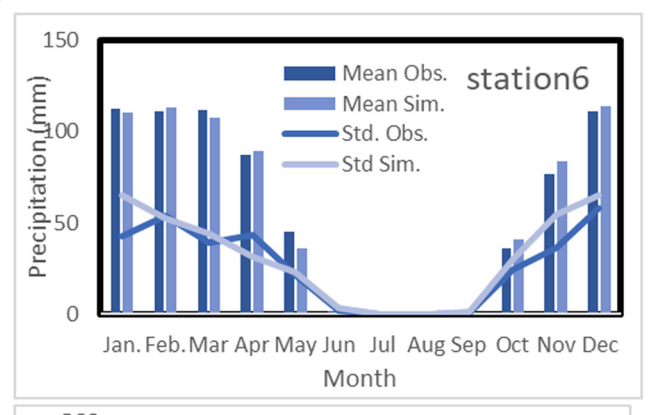
DE GRUYTER

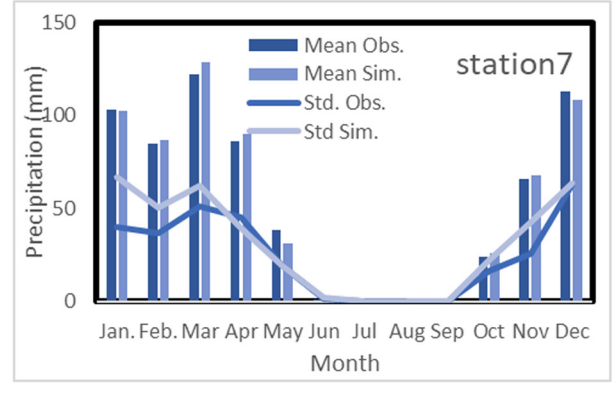












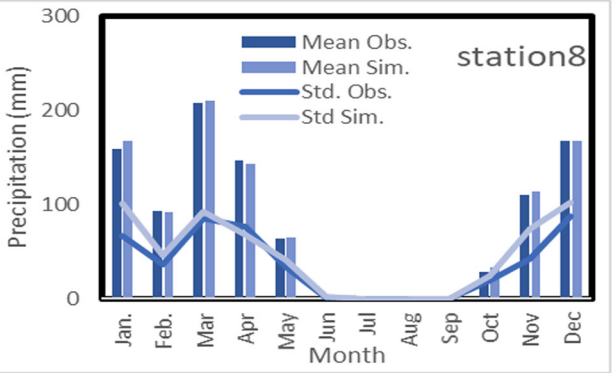


Figure 2: (Continued)

Table 5: Statistical parameter results for calibration and validation of the LARS-WG model over the baseline period (2001–2020)

Station name	Climate variable	R ²	N _{SE}	RSR
Station 1	Max. temp.	0.9996	0.9996	0.0203
	Min. temp	0.9994	0.9993	0.0256
	Precipitation	0.9955	0.9952	0.0694
Station 2	Max. temp.	0.9994	0.9994	0.0246
	Min. temp	0.9995	0.9995	0.0225
	Precipitation.	0.9886	0.9864	0.1164
Station 3	Max. temp.	0.9993	0.9993	0.0266
	Min. temp	0.9992	0.9991	0.0292
	Precipitation.	0.9871	0.9864	0.1163
Station 4	Max. temp.	0.9993	0.9993	0.0261
	Min. temp	0.9994	0.9992	0.0278
	Precipitation.	0.9953	0.9876	0.111
Station 5	Max. temp.	0.9993	0.9993	0.0266
	Min. temp	0.9995	0.9994	0.0244
	Precipitation.	0.9881	0.9852	0.1214
Station 6	Max. temp.	0.9994	0.9993	0.0256
	Min. temp	0.9995	0.9994	0.0236
	Precipitation.	0.9931	0.9930	0.0839
Station 7	Max. temp.	0.9995	0.9994	0.0233
	Min. temp	0.9995	0.9995	0.0218
	Precipitation.	0.9947	0.9943	0.0753
Station 8	Max. temp.	0.9995	0.9995	0.0223
	Min. temp	0.9995	0.9995	0.0228
	Precipitation.	0.9983	0.9978	0.0470

$$N_{\rm SE} = 1 - \frac{\sum_{i=1}^{N} (Q_i - M_i)^2}{\sum_{i=1}^{N} (Q_i - Q_i)^2},$$
 (5)

RSR =
$$\frac{\text{RMSE}}{\text{STD}_{\text{ob}}} = \frac{\sqrt{\sum_{i=1}^{N} (Q_i - M_i)^2}}{\sum_{i=1}^{N} (Q_i - Q_2)^2}$$
. (6)

where Q_i and M_i are the observed and simulated stream flow values for the ith pair of stream flow values, respectively. Q_a is the mean value of the observed stream flow values, N is the total number of paired stream flow values, and M_a is the mean value of the modeled stream flow.

4 Results and discussion

4.1 LARS-WG model calibration and validation

In this study, daily climate variables (i.e., precipitation, maximum temperature, and minimum temperature) for eight stations in the study area were collected for 20 years as a reference period from 2001–2020 in calibrating and

validating the LARS-WG model. The calibration and validation process can be summarized in two steps as follows: (1) using the ANALYSE SITE window, the daily observed meteorological data (precipitation, maximum and minimum temperatures, and solar radiation) of the Mosul Dam watershed are analyzed to compute their statistical parameters and save these data to two separate parameters files; (2) from two parameter files derived in step (1), the statistical parameters of eight weather stations were automatically calculated by LARS-WG version 6.0 as a TST file after using the generated data in the generation process. Table 3 outlines the statistical analysis of the measured seasonal climate variable data (precipitation, maximum, and minimum temperatures) within the validation process. Similarly, the statistical analysis for the observed monthly precipitation within the same process is shown in Table 4. The value of N in each table indicates the total number of tests performed.

To sum up, the model performs well in assessing the wet and dry series distributions. All stations had either a perfect fit or a very good fit throughout the winter: December, January, February (DJF); autumn: September, October, November (SON); spring: March, April, May (MAM); and a poor to very good fit was found during the summer evaluation: June, July, August (JJA). According to Table 4, the model's performance ranges from very good to perfect when simulating daily rain distributions, except in the summer; the value of N in each table indicates the total number of tests performed. According to Table 4, the model's performance ranges from good to perfect when simulating daily rain distributions, except in the summer; the model cannot adjust for dry periods and accurately assess the weather due to the lack of precipitation during the dry season.

To validate the model's prediction of future climate variables at all locations, the mean value and standard deviation of two climate variable series (observed and generated) for all stations in this study were compared for each month, as illustrated in Figure 2.

Considering how challenging it has been to model standard deviations satisfactorily in previous studies, the results are generally encouraging. Figure 2 shows the model's adequate record for predicting monthly averages and standard deviations for minimum and maximum temperatures across all locations. In addition, the model's ability to predict low and high temperatures and precipitation would confirm what was previously discussed. This verifies the tool's applicability across all areas in the current study and suggests it could be used elsewhere to predict future daily weather values.

The results for all stations' average monthly values of Tmax, Tmin, and precipitation are shown in Table 5, along

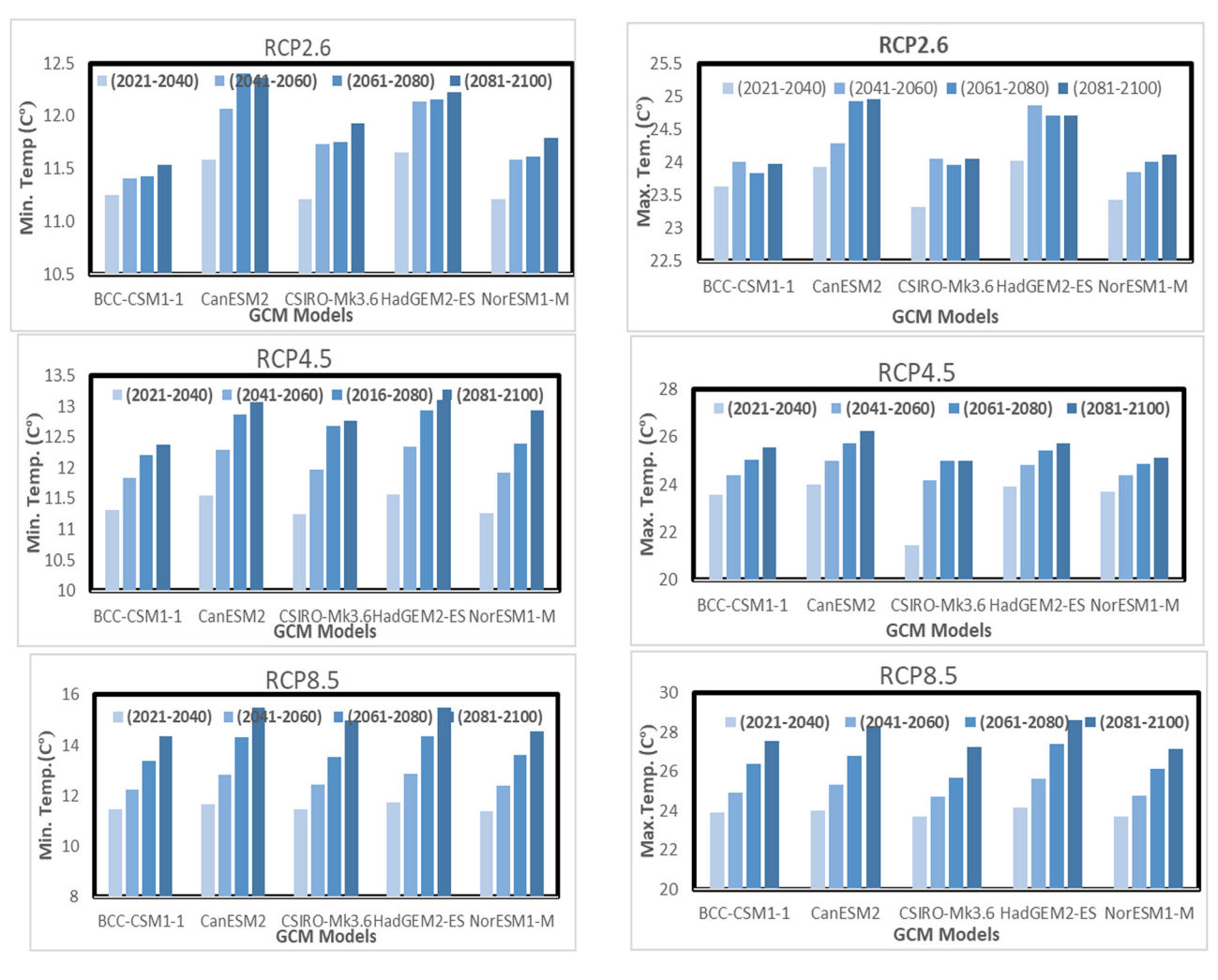


Figure 3: Projected minimum and maximum temperatures for four periods for all scenarios for GCM models.

with the coefficient of determination (R^2), $N_{\rm SE}$, and RSR. Across all study stations, statistical indicators showed a high concordance between observed and down-scaled data from the downscaling model. As a result, all eight climate variables had a high coefficient of determination (R^2) and Nash–Sutcliffe coefficient values, between 0.9871 and 0.9996, and between 0.9996 and 0.9864, respectively, and low RSR between 0.0203 and 0.1214.

4.2 Future trends in climate variables

The calibrated weather generator model for all stations was utilized to project the observed min. temp., max. temp., and precipitation in the baseline period (2001–2020) onto (2021–2040), (2041–2060), (2061–2080), and (2081–2100). This study employed various scenarios of greenhouse gas emissions, namely, RCP2.6, RCP4.5, and RCP8.5. In addition, it utilizes five GCMs, reviewed in Table 2, to downscale the

climate variables for the watershed. Finally, the watershed's projected minimum and maximum temperatures are plotted as shown in Figures 3 and 4.

Figure 3 shows the simulated maximum and minimum temperatures concerning the GCM models for four periods under three greenhouse gas emission scenarios. It is clear from Figure 3 that there is a discrepancy in predicting the future minimum and maximum temperatures for each of the climate change models. The highest future prediction of these climate variables was those extracted from the CanESM2 model, then the HadGEM2-ES model, while the lowest future forecast was from the CSIRO-Mk3.6 model for all scenarios of greenhouse gas emissions. For this reason, the future change in minimum, maximum, and precipitation for the study area was calculated according to the mean value of five GCM model results.

The predicted average monthly minimum and maximum temperatures over the four time periods are displayed in Figure 4. Figure 4 shows that most of the average

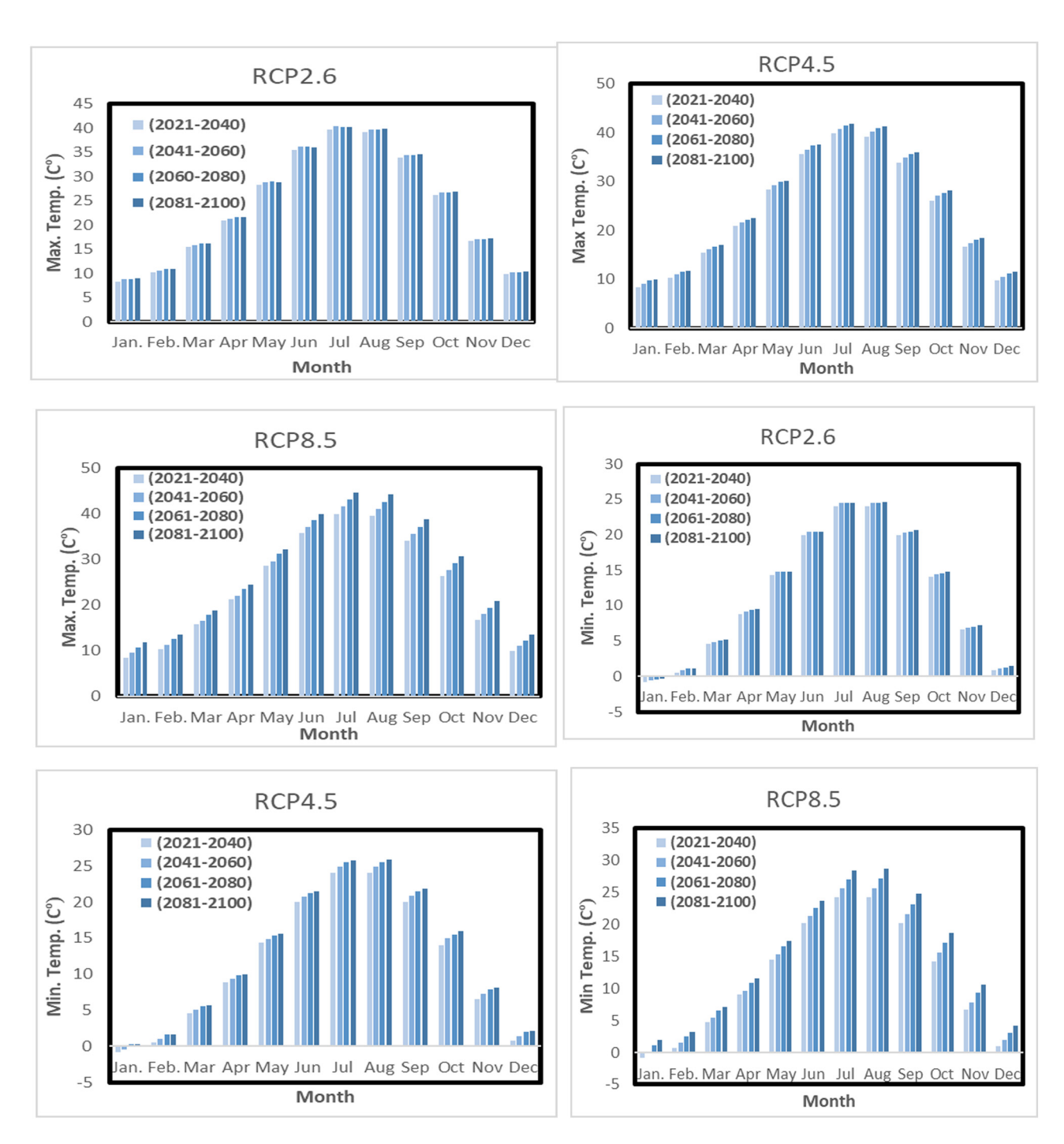


Figure 4: Future maximum and minimum temperatures for all periods under three climate change scenarios.

monthly maximum temperature has risen in the summer months of July, August, and September, while the least of it has risen in the winter months of December and January. Minimum and maximum temperatures gradually increase between the observed values for 2001–2020 and those predicted by this century's end for all future scenarios. These results agreed with that reported by Mohammed and Hassan [1].

The average monthly differences in minimum and maximum temperatures for all future periods under three scenarios of climate change are illustrated in Figure 5. The highest difference (increase) in maximum and minimum temperatures was 5.70°C in July and 5.30°C in September, respectively for the future period (2081–2100) under RCP8.5. In contrast, the lowest difference (increase) in maximum and minimum temperatures were 0.16°C and 0.05°C in

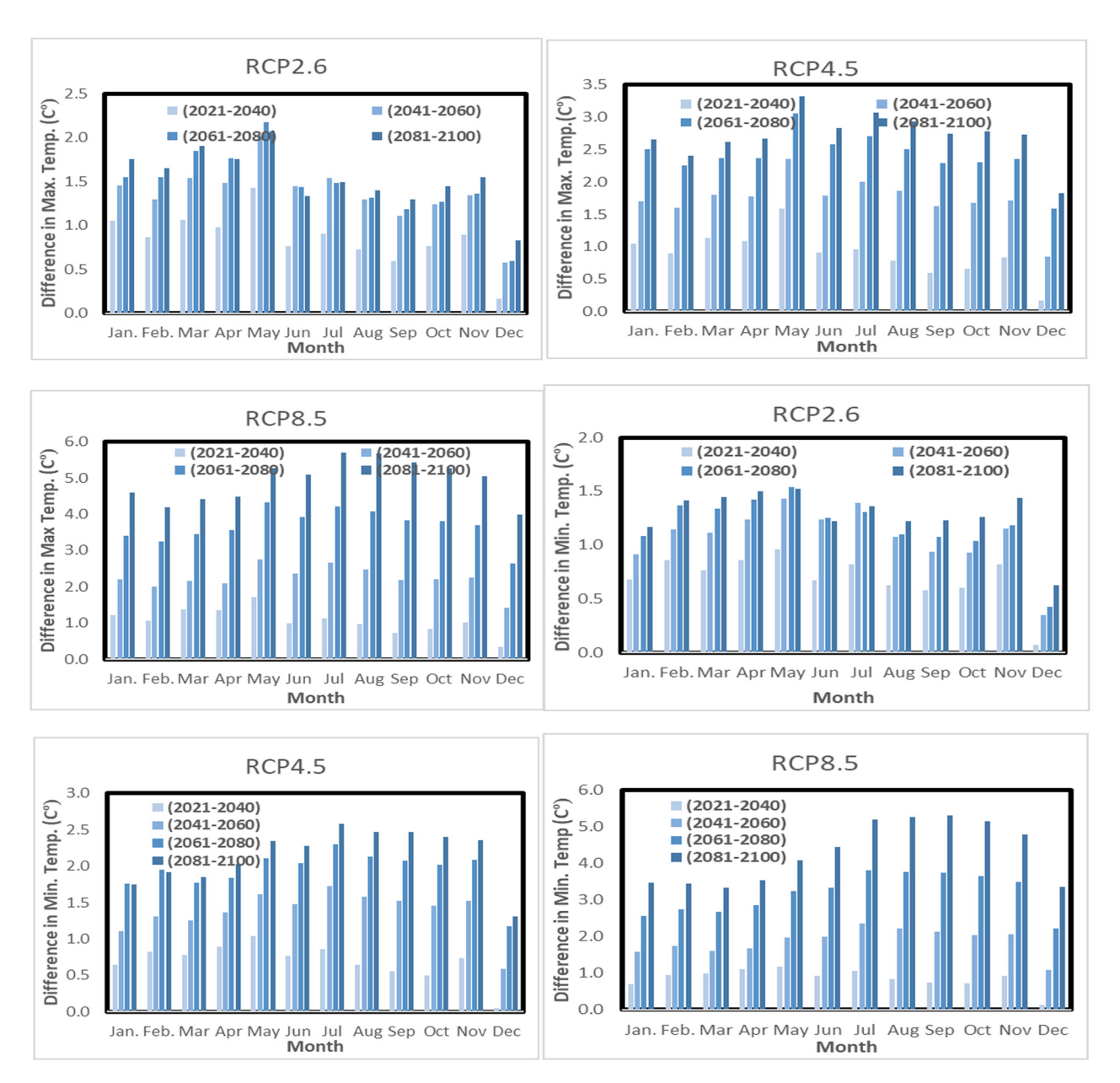
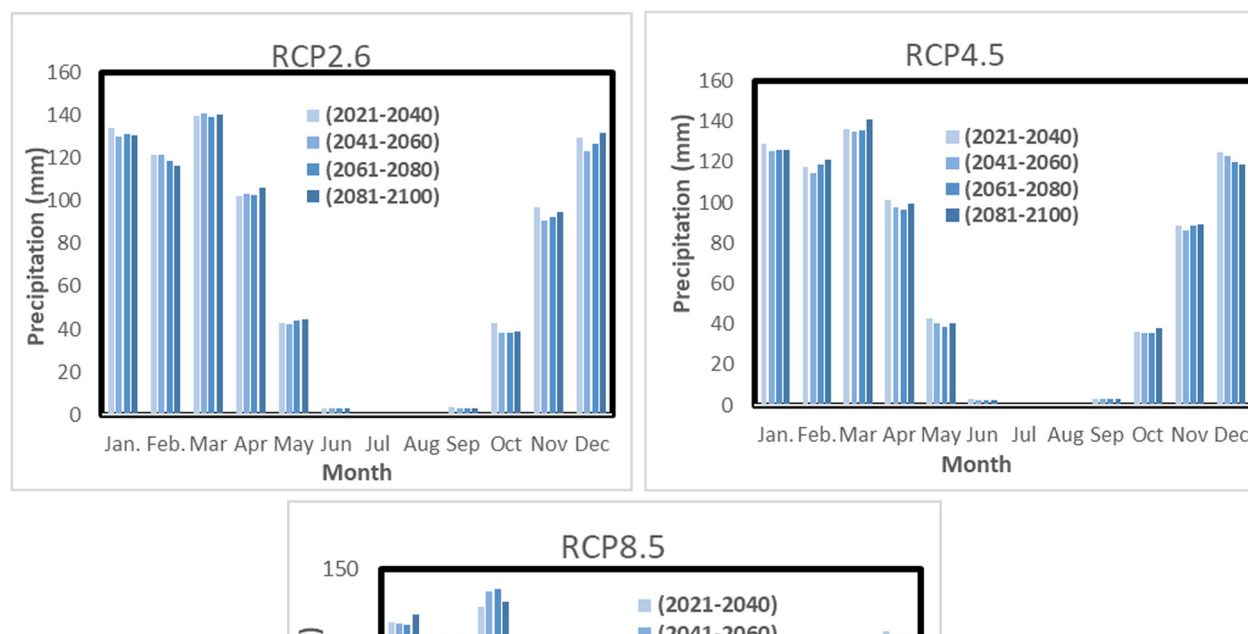


Figure 5: Average monthly differences in maximum and minimum temperature for all future periods under three climate change scenarios.

December for the future period (2021–2040) under the greenhouse gas emission scenarios RCP2.6 and RCP4.5.

The prediction of precipitation for each scenario is depicted in Figure 6. However, it can be observed that there are variations in the projected precipitation values between each scenario throughout all periods in the future. These variations are because rainfall does not occur continuously during the year. As a result, there are missing values for some months, which makes it challenging to forecast rainfall for the upcoming months.

Figure 7 shows the precipitation trend averaged from the five GCMs across the entire watershed. In general, it can be seen that the future change in the precipitation has fluctuated between increases and decreases, e.g., example, under the RCP2.6 scenario, the highest increase was found to be 16 mm in November for the period (2021–2040), while for the same scenario, the highest decrease was found to be 8.9 mm in May for the period (2041–2060). Therefore, it is reasonable to infer that the North of Iraq will experience different patterns of precipitation change during the wet



RCP8.5

(2021-2040)
(2041-2060)
(2061-2080)
(2081-2100)

Jan. Feb. Mar Apr May Jun Jul Aug Sep Oct Nov Dec Month

Figure 6: Average monthly future precipitation for four periods under three climate change scenarios.

seasons in the future periods. Furthermore, the presented results were consistent with those reported by Osman et al. [3].

The study demonstrated that the evaluated watershed would witness an increase in the trend of maximum and minimum temperatures. For example, the stations located within the Turkish borders will witness an increase in maximum and minimum temperatures more than those located within the Iraqi borders under all climate change scenarios and for all study periods. This is due to several factors, including the topography and geography of the area where the topography of an area can significantly influence its temperature. Turkish regions may have higher elevations than Iraqi regions, and temperature changes tend to be more pronounced at higher altitudes. As the climate warms, this elevation effect can lead to amplified temperature increases in Turkish areas. On the other hand, precipitation in the region will witness a slight increase across the entire watershed, regardless of the position of the stations inside or outside Iraq (Table 6).

5 Conclusion

This study tested the weather generator model (LARS-WG) application to downscale the daily climate variables, including maximum and minimum temperatures and precipitation in the north of Iraq (Mosul Dam watershed, which includes many regional areas). Subsequently, the model was utilized in generating the future daily climate variables for four periods (2021–2040), (2041–2060), (2061–2080), and (2081–2100) under three scenarios of greenhouse gas emission RCP2.6, RCP4.5, and RCP8.5. In addition, the observed daily climate variable data for the period (2001–2020) were used to calibrate and validate the weather generator model and compared with the future period's data. From the analysis of the model in this study, it can be concluded that:

 LARS-WG is a statistical downscaling method. It can relate large-scale predictors with the local climate variables like rainfall and temperatures.

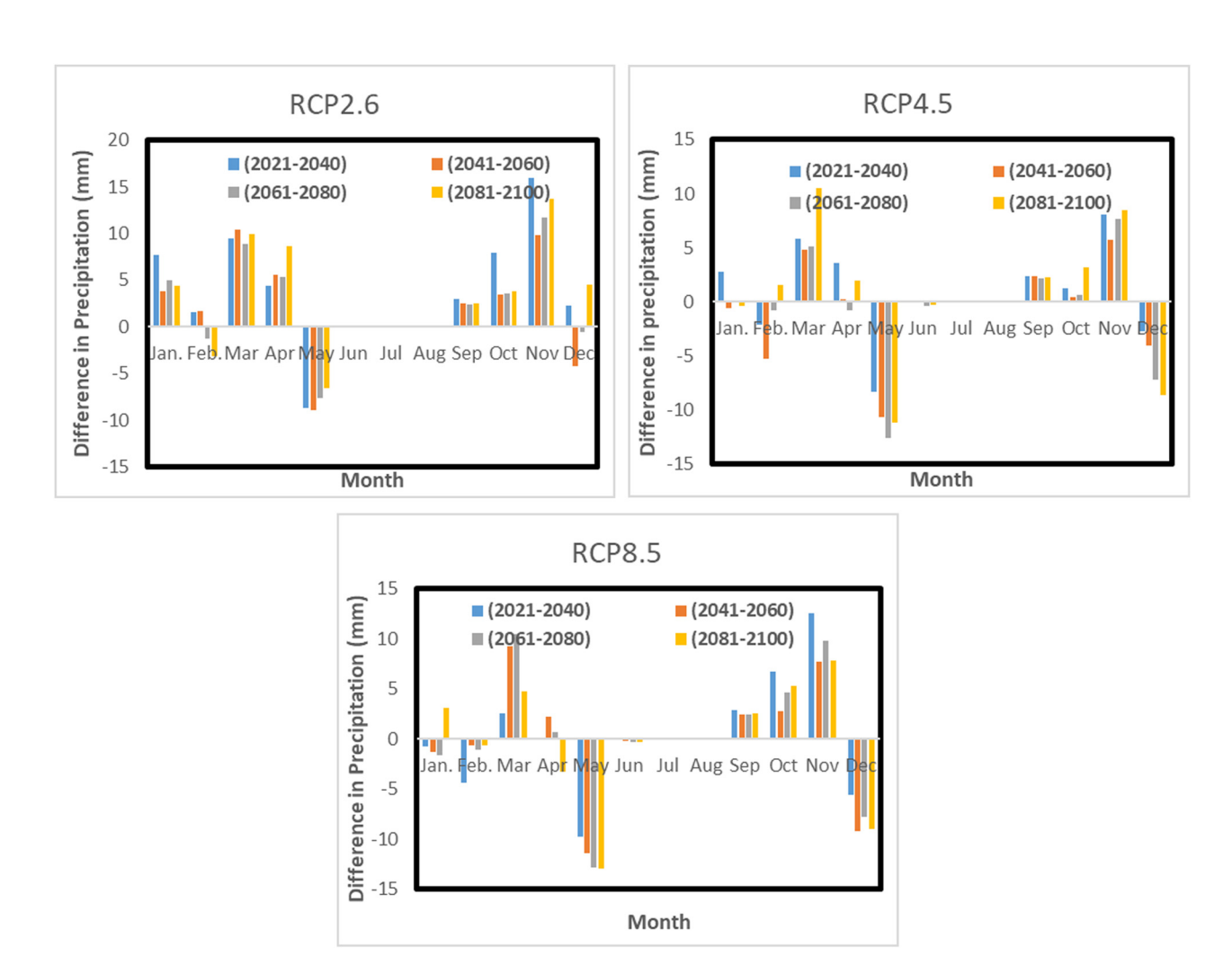


Figure 7: Average monthly difference in precipitation for four periods under three scenarios of climate change.

DE GRUYTER

Table 6: Change in climate variables under corresponding scenarios in the study according to the position of the station

Scenario	Period	Change in Turkey	stations		% change in Iraq stations			
		Max. temp. (°C)	Min. temp. (°C)	% prec.	Max. temp. (°C)	Min. temp. (°C)	% prec.	
RCP2.6	2021-2040	0.81	0.61	7.34	0.63	0.78	7.43	
	2041-2060	1.36	1.00	4.58	1.04	1.33	7.48	
	2061-2080	1.45	1.11	4.40	1.11	1.40	7.73	
	2081-2100	1.52	1.20	5.43	1.21	1.47	8.22	
RCP4.5	2021-2040	0.54	0.62	3.61	0.63	0.82	3.90	
	2041-2060	1.72	1.30	0.12	1.32	1.66	2.50	
	2061-2080	2.39	1.84	0.49	1.87	2.32	2.78	
	2081-2100	2.69	2.07	3.34	2.10	2.66	3.66	
RCP8.5	2021-2040	1.04	0.76	3.61	0.80	0.99	3.70	
	2041-2060	2.23	1.78	2.61	1.81	2.18	2.89	
	2061-2080	3.63	3.03	2.12	3.10	3.58	4.47	
	2081-2100	4.92	4.18	1.07	4.23	4.87	3.38	

- 2. The study has a limited number of weather stations which affect the accuracy of the prediction of climate data.
- 3. The results obtained by increasing the temperature will negatively influence water and food security in Iraq.
- 4. This study's main finding can help assess the potential risks and challenges associated with changes in water availability, agricultural practices, and ecological balance. Moreover, this research provides valuable information for policymakers, water resource managers, and local communities who can benefit from the findings to develop strategies to adapt to and mitigate future climate change impacts in northern Iraq.

Funding information: Authors declare that the manuscript was done depending on the personal effort of the authors, and there is no funding effort from any side or organization.

Conflict of interest: The authors state no conflict of interest.

Data availability statement: Most datasets generated and analyzed in this study are comprised in this submitted manuscript. The other datasets are available on reasonable request from the corresponding author with the attached information.

References

- [1] Mohammed ZM, Hassan WH. Climate change and the projection of future temperature and precipitation in southern Iraq using a LARS-WG model. Model Earth Syst Environ. 2022;8(3):4205–18. doi: 10.1007/s40808-022-01358-x.
- [2] Kavwenje S, Zhao L, Chen L, Chaima E. Projected temperature and precipitation changes using the LARS-WG statistical downscaling model in the Shire River Basin, Malawi. Int J Climatol. 2021;42(1):400–15. doi: 10.1002/joc.7250.
- [3] Osman Y, Al-Ansari N, Abdellatif M, Aljawad SB, Knutsson S. Expected future precipitation in central Iraq using LARS-WG Stochastic Weather Generator. Engineering. 2014;06(13):948–59. doi: 10.4236/enq.2014.613086.
- [4] Al-Mukhtar M. Modeling of pan evaporation based on the development of Machine Learning Methods. Theor Appl Climatol. 2021;146(3–4):961–79. doi: 10.1007/s00704-021-03760-4.
- [5] Al-Kakey O, Al-Mukhtar M, Berhanu S, Dunger V. Assessing CFSR climate data for rainfall-runoff modeling over an ungauged basin between Iraq and Iran. Kuwait J Sci. 2023;50(3):405–14. doi: 10. 1016/j.kjs.2022.12.004.
- [6] Lionello P, Scarascia L. The relation between climate change in the Mediterranean region and global warming. Reg Environ Change. 2018;18(5):1481–93. doi: 10.1007/s10113-018-1290-1.
- [7] Touzé-Peiffer L, Barberousse A, Le Treut H. The coupled model intercomparison project: History, uses, and structural effects on

- climate research. WIREs Clim Change. 2020;11(4):1–15. doi: 10.1002/wcc.648.
- [8] Al-Ansari N, Abdellatif M, Ali S, Knutsson S. Long term effect of climate change on rainfall in Northwest Iraq. Open Eng. 2014;4(3):250–63. doi: 10.2478/s13531-013-0151-4.
- [9] Shiogama H, Stone D, Emori S, Takahashi K, Mori S, Maeda A, et al. Predicting future uncertainty constraints on global warming proiections. Sci Rep. 2016;6(1):1–7. doi: 10.1038/srep18903.
- [10] Hansen JW, Mavromatis T. Correcting low-frequency variability bias in stochastic weather generators. Agric For Meteorol. 2001;109(4):297–310. doi: 10.1016/s0168-1923(01)00271-4.
- [11] Araya A, Prasad PVV, Gowda PH, Djanaguiramana M, Gebretsadkan Y. Modeling the effects of crop management on food barley production under a midcentury changing climate in northern Ethiopia. Clim Risk Manag. 2021;32:100308. doi: 10.1016/j.crm.2021.100308.
- [12] Hamlet AF, Byun K, Robeson SM, Widhalm M, Baldwin M. Impacts of climate change on the State of Indiana: Ensemble future projections based on statistical downscaling. Clim Change. 2019;163(4):1881–95. doi: 10.1007/s10584-018-2309-9.
- [13] Tang J, Niu X, Wang S, Gao H, Wang X, Wu J. Statistical downscaling and dynamical downscaling of regional climate in China: Present climate evaluations and future climate projections. J Geophys Res: Atmos. 2016;121(5):2110–29. doi: 10.1002/2015jd023977.
- [14] Birara H, Pandey RP, Mishra SK. Projections of future rainfall and temperature using statistical downscaling techniques in Tana Basin, Ethiopia. Sustain Water Resour Manag. 2020;6(5):1–17. doi: 10.1007/s40899-020-00436-1.
- [15] Al-Mukhtar M, Dunger V, Merkel B. Evaluation of the climate generator model CLIGEN for rainfall data simulation in Bautzen catchment area, Germany. Hydrol Res. 2013;45(4–5):615–30. doi: 10.2166/nh.2013.073.
- [16] Kareem HH, Alkatib AA. Future short-term estimation of flowrate of the Euphrates River catchment located in Al-Najaf Governorate, Iraq through using weather data and statistical downscaling model. Open Eng. 2022;12(1):129–41. doi: 10.1515/eng-2022-0027.
- [17] Whitehead PG, Barbour E, Futter MN, Sarkar S, Rodda H, Caesar J, et al. Impacts of climate change and socio-economic scenarios on flow and water quality of the Ganges, Brahmaputra and Meghna (GBM) river systems: Low flow and flood statistics. Environ Sci: Process Impacts. 2015;17(6):1057–69. doi: 10.1039/c4em00619d.
- [18] Haitham L, Al-Mukhtar M. Assessment of future climate change impacts on water resources of Khabour River catchment, north of Iraq. Eng Technol J. 2022;40(5):695–709. doi: 10.30684/etj.v40i5.1925.
- [19] Munawar S, Rahman G, Moazzam MF, Miandad M, Ullah K, Al-Ansari N, et al. Future climate projections using SDSM and LARS-WG downscaling methods for CMIP5 GCMS over the transboundary Jhelum river basin of the Himalayas region. Atmosphere. 2022;13(6):898. doi: 10.3390/atmos13060898.
- [20] Mohammed R, Scholz M. Climate change and water resources in arid regions: Uncertainty of the baseline time period. Theor Appl Climatol. 2018;137(1–2):1365–76. doi: 10.1007/s00704-018-2671-6.
- [21] Zakaria S, Al-Ansari N, Knutsson S. Historical and future climatic change scenarios for temperature and rainfall for Iraq. J Civ Eng Architecture. 2013;7(12):1574–94. doi: 10.17265/1934-7359/2013.12.012.
- [22] Racsko P, Szeidl L, Semenov M. A serial approach to local stochastic weather models. Ecol Model. 1991;57(1–2):27–41. doi: 10.1016/0304-3800(91)90053-4.
- [23] Semenov M, Brooks R. Spatial interpolation of the LARS-WG stochastic weather generator in Great Britain. Clim Res. 1999;11:137–48. doi: 10.3354/cr011137.

- [24] Semenov M, Brooks R, Barrow E, Richardson C. Comparison of the WGEN and LARS-WG stochastic weather generators for diverse climates. Clim Res. 1998;10:95-107. doi: 10.3354/ cr010095.
- [25] Katz RW. Use of conditional stochastic models to generate climate change scenarios. Clim Change. 1996;32(3):237-55. doi: 10.1007/
- [26] Santhi C, Arnold JG, Williams JR, Dugas WA, Srinivasan R, Hauck LM. Validation of the SWAT model on a large RWER basin with point and
- nonpoint sources. J Am Water Resour Assoc. 2001;37(5):1169-88. doi: 10.1111/j.1752-1688.2001.tb03630.x.
- [27] Van Liew MW, Arnold JG, Garbrecht JD. Hydrologic simulation on agricultural watersheds: choosing between two models. Trans ASAE. 2003;46(6):1539.
- [28] Moriasi DN, Arnold JG, Van Liew MW, Bingner RL, Harmel RD, Veith TL. Model evaluation guidelines for systematic quantification of accuracy in watershed simulations. Trans ASABE. 2007;50(3):885-900.